Nanoscale

Accepted Manuscript

Nanoscale

Volume 10
Number 4
28 January 2018
Pages 1549-2172

rsc.li/nanoscale

ISSN 2040-3372

PAPER
Shuping Xu, Chongyang Liang et al.
Organelle-targeting surface-enhanced Raman scattering
(SERS) nanosensors for subcellular pH sensing

ROYAL SOCIETY
OF CHEMISTRY

NCNST

ROYAL SOCIETY
OF CHEMISTRY

rsc.li/nanoscale

ARTICLE

Biomass-derived substrates hydrogenation over Rhodium Nanoparticles Supported on Functionalized Mesoporous Silica

Israel T. Pulido-Díaz[a,b], Draco Martínez[a], Karla P. Salas-Martin[a], Benjamín Portales-Martínez[d], Dominique Agustin[b,c], Antonio Reina[a], and Itzel Guerrero-Ríos[a*]

The use of supported rhodium nanoparticles (RhNPs) is gaining attention due to the drive for better catalyst performance and sustainability. Silica-based supports are promising for RhNP immobilization because of their thermal and chemical stability. Functionalizing silica allows for the design of catalysts with improved activity for biomass transformations. In this study, we synthesized Rhodium nanoparticles (RhNPs) supported on N-functionalized silica-based materials, utilizing SBA-15 as the support and functionalizing it with either nicotinamide or imidazolium-based ionic liquid. Solid-state ^{29}Si and ^{13}C NMR experiments confirmed successful ligand anchoring onto the silica surface. RhNPs@SBA-15-Imz[NTf$_2$] and RhNPs@SBA-15-NIC were efficiently prepared and extensively characterized, revealing small, spherical, and well-dispersed fcc Rh nanoparticles on the support surface, confirmed by XPS analyses detecting metallic rhodium, Rh(I), and Rh(III) species. The catalytic performance of these materials is assessed in the hydrogenation of biomass-derived substrates, including furfural, levulinic acid, terpenes, vanillin, and eugenol, among others, underscoring their potential in sustainable chemical transformations. The nanocatalysts demonstrated excellent recyclability and resistance to metal leaching over multiple cycles. The study shows that neutral and ionic silica grafting fragments differently stabilize RhNPs, affecting their morphology, size, and interaction with silanol groups, that impact their catalytic activity.

Introduction

The depletion of non-renewable fossil resources and the increase of environmental pollution have compelled the scientific community to focus on sustainable concepts, especially for production and use of renewable chemicals.[1] Biomass, as the organic carbon source on Earth, holds a significant importance in this regard.[2,3] Lignocellulosic biomass is the primary component of non-edible biomass, composed mainly of lignin, cellulose, hemicellulose, and lignocellulose. Lignin is the biopolymer that constitutes the main source of aromatics in nature.[4-7] Consequently, conversion of lignin into chemicals, fuels, and carbon-based functional materials has become a topic of great importance.[8,9] In this context, lignin upon depolymerization produces phenolic monomers, which can be hydrogenated to access added-value oxygenated molecules, representing an interesting strategy to valorize biomass.[6,10-14] As an example, the valorization of lignin derived phenol through hydrogenation produced cyclohexanone and cyclohexanol,[25,26] which are intermediates for the synthesis of caprolactam and adipic acid, both key materials for the industrial production of nylon.[30] One of the main issues during these processes is the lack of selectivity, due to the formation of several side-products. Starting from complex carbohydrates like starch, cellulose, and hemicellulose, we can easily get oxygen-rich materials and convert them into renewable building blocks.[15] Reduction of substrates like furan-based substrates,[10] levulinic acid, [16-22] 5-hydroxymethylfurfural, [23, 24] sorbitol, and others,[27-29] facilitates the production of biofuels and important intermediates in the synthesis of fine chemicals. Rhodium-based catalysts favor a wide range of chemical transformations, including hydrogenations, hydroformylations, and carbonylations, [31-34] finding applications in various industrial processes. From a sustainable context, catalysts are required to perform under mild conditions, but also to enhance catalyst performance especially through its prolonged shelf-life through reuse and recycling. Supported rhodium nanoparticles (RhNPs) fulfilled these requirements.[6] RhNPs have been successfully supported in various ways, including liquid phases such as ionic liquids,[35] and glycerol,[36,37] or solid phases, including activated carbon,[41,42] alumina,[43] polystyrene [44] and silica.[38-40] Silica-based supports offer thermal and chemical stability for catalysts and present a wide morphology diversity. In addition, functionalization of silica with coordinating molecules enables the immobilization of molecular catalysts

a. *Departamento de Química Inorgánica y Nuclear, Facultad de Química, UNAM, Circuito Escolar S/N, Coyoacán, Cd. Universitaria, 04510 Ciudad de México, México. E-mail: itzelgr@unam.mx*

b. *Centre National de la Recherche Scientifique (CNRS), Laboratoire de Chimie de Coordination (LCC), Université de Toulouse, UPS, INPT, 205, route de Narbonne, 31077 Toulouse, France.*

c. *Université de Toulouse, IUT P. Sabatier, Département de Chimie, Av. G. Pompidou, BP 20258, 81104 Castres CEDEX, France*

d. *CONACYT, Centro de Investigación en Ciencia Aplicada y Tecnología Avanzada, Laboratorio Nacional de Conversión y Almacenamiento de Energía, Instituto Politécnico Nacional, Calzada Legaría 694, Col. Irrigación, Ciudad de México, 11500, México*

† Electronic Supplementary Information (ESI) available: Characterization spectra of Silicas (TGA, IR, BET, NMR), RhNPs (IR, TGA, BET, SEM, TEM, XPS, EDX), Tables of selected catalytic reactions, and NMR of products See DOI: 10.1039/x0xx00000x

Nanoscale Accepted Manuscript

ARTICLE

and metal nanoparticles, through interaction between catalytically active objects and modified supports.[45-51]
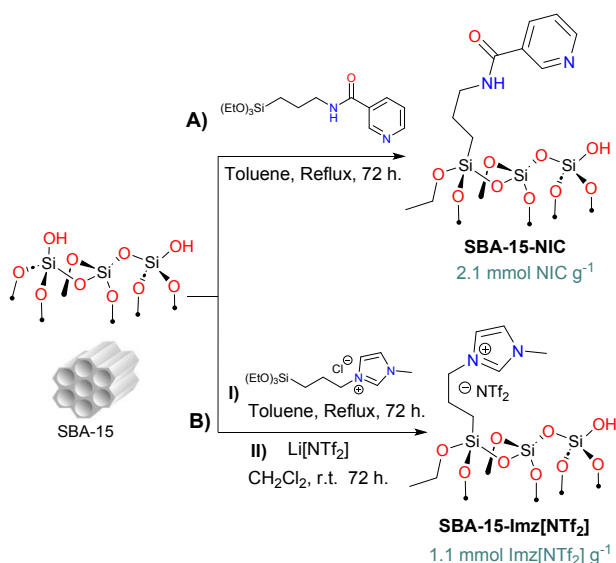
Scheme 1. Synthesis of functionalized silica-based supports. A) SBA-15-NIC; B) SBA-15-Imz[NTf$_2$].

Indeed, functionalization permits a rational design and tuning of silica-based materials, yielding novel materials with higher activity for biomass transformations.[52] In our group, we have shown recently that RhNPs supported on *N*-functionalized MCM-41 silica facilitates the hydrogenation of several functional groups, including challenging substrates such as quinolines, nitriles, phenol, aldehydes, and ketones, under mild conditions.[53] In addition, bare MCM-41 does not stabilize RhNPs and agglomerates of rhodium nanoparticles does not compare in activity nor selectivity with the catalysts supported on N-functionalized MCM-41. Herein, rhodium nanoparticles supported on SBA-15 functionalized with nicotinamide, and imidazolium-based ionic liquid are studied, from synthesis and characterization to its catalytic evaluation in the hydrogenation of biomass-derived substrates including furfural, levulinic acid, terpenes, vanillin, and eugenol, among others.

Results and Discussion

Catalyst Synthesis and Characterization

Organo(triethoxy)silane derivatives bearing nicotinamide (NIC) or imidazolium salt (Imz[NTf$_2$]) as terminal function were grafted on silica through silanization (**Scheme 1**) using classical methods.[54,55]

FT-IR (ATR) analysis of silica-based materials (Figure S1) showed typical signals of the silica backbone (siloxane, silanol groups, and physisorbed water). For SBA 15-Imz[NTf$_2$] distinct signals corresponding to the imidazole ring (1574 cm^{-1}) and bistriflimide anion (1345 cm^{-1}, 1184 cm^{-1}, and 952 cm^{-1}) were identified.[56] For SBA 15-NIC, a prominent band was observed at around 1646 cm^{-1}, indicative of the stretching vibration of the amide carbonyl group, along with a minor signal at 1545 cm^{-1} corresponding to the N-H bending vibration.[53] The amount of

ligand grafted on SBA-15 was determined through thermogravimetric analysis and elemental analysis obtaining ca. 33% and 25% wt. for SBA 15-Imz[NTf$_2$] and SBA 15-NIC respectively (Figure S5).

Solid-state ^{29}Si and ^{13}C NMR spectroscopies provided extra information about the degree of functionalization with either nicotinamide (NIC) or imidazolium salt (Imz[NTf$_2$]). ^{29}Si UDEFT (Uniform Driven Equilibrium Fourier Transform) technique [57] was selected to perform quantitative one-dimensional ^{29}Si NMR experiments under magic-angle spinning (MAS) conditions. The NMR spectra of functionalized silica materials, (Figure 1) display three distinct resonances at -94 ppm (Q^2), -102 ppm (Q^3) and -111 ppm (Q^4), which correspond to the silica backbone. Additionally, two other resonances at -57 ppm (T^2) and at -67 ppm (T^3) are attributed to the grafted organosiloxanes.[58] The prevalence of T^n peaks over Q^n confirms that the ligands are effectively condensed as a part of the silica framework.[59] The deconvolution of quantitative ^{29}Si NMR spectra allows for the estimation of silane grafting percentages, which are found to be 11.4% for SBA-15-Imz[NTf$_2$] and 12.9% for SBA-15-NIC. Furthermore, the integration of multiple techniques, including elemental analysis, thermogravimetric analysis, and adsorption/desorption isotherms, in conjunction with ^{29}Si NMR, enables the calculation of surface coverage by ligands. (See ESI Table S1) This analysis reveals approximately 2.4 and 3.9 molecules per nm² for SBA-15-Imz[NTf$_2$] and SBA-15-NIC, respectively. These findings indicate that the grafting process is significantly influenced by the type of organic moiety on the silane, with the NIC moiety leading to greater surface coverage on the silica material.
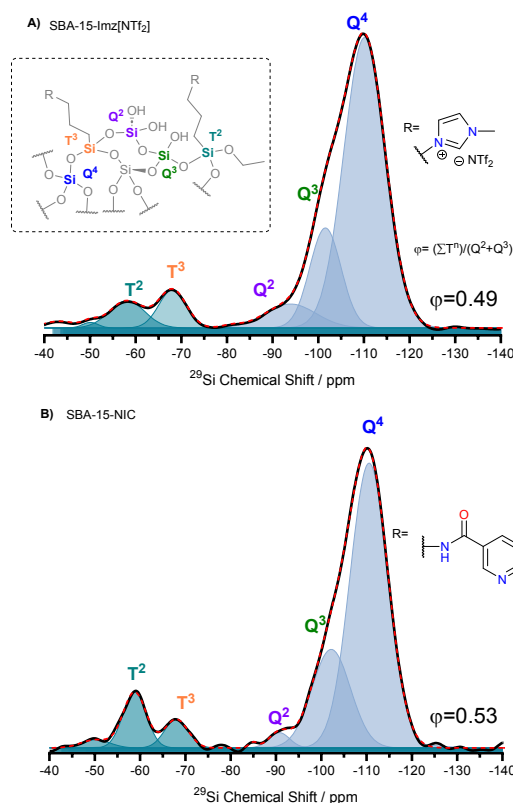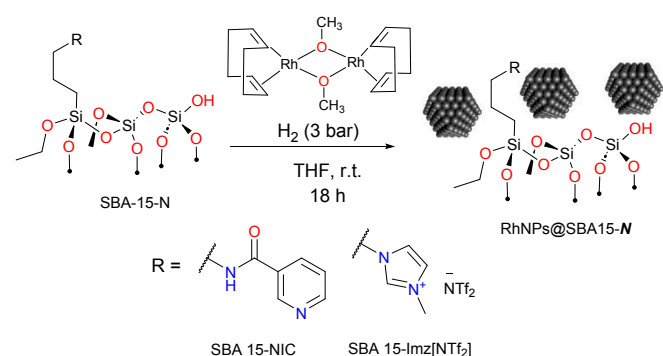
Figure 1. (**A**) ^{29}Si UDEFT-MAS NMR spectra of SBA-15-Imz[NTf$_2$] (**B**) and SBA-15-NIC. Inset: Schematic representing surface grafting possibilities for organosiloxanes on silica

Scheme 2. General synthesis of RhNPs@SBA-15-*N*.

^{13}C CP-MAS NMR spectra confirmed the presence of the corresponding ligand for each material (Figure S8). Characteristic signals corresponding to the imidazole ring (134.6 ppm, 120.9 ppm, and 34.9 ppm), and to the nicotinamide moiety (165 ppm, and 123-147 ppm) were observed for SBA-15-Imz[NTf$_2$] and SBA-15-NIC, respectively.

The as-prepared materials were employed for Rhodium nanoparticles immobilization. RhNPs were obtained through decomposition of the organometallic precursor methoxy (cyclooctadiene) rhodium(I) dimer [Rh(μ-OMe)(1,5-COD)]$_2$, under hydrogen pressure (Scheme 2). Nanoparticles were synthesized under mild conditions (3 bar of H$_2$ at room temperature) in presence of functionalized SBA 15-N, yielding air-stable black powders containing 10 wt. % of Rh. Far-IR spectroscopy showed a characteristic signal at 462 cm^{-1} corresponding to a rhodium-nitrogen stretching vibration, pointing out the coordination of metal nanoparticles to the grafted ligand (Figure S4).[60]

High-angle annular dark-field scanning transmission electron microscopy (HAADF-STEM) of the supported RhNPs showed pseudo-spherical, small, and well-dispersed particles for both materials (Figure 3). RhNPs@SBA-15-Imz[NTf$_2$] and RhNPs@SBA-15-NIC showed very small nanoparticles with a mean diameter of 2.7 ± 0.6 nm, and 1.7 ± 0.3 nm, respectively. In both cases, nanoparticles were located at the surface and in the pores of the functionalized silica-based support, and narrow-size distributions were obtained. STEM images together with electronic diffraction analysis and fast-Fourier-transform evidenced the face centered cubic (fcc) crystalline structure of metallic Rh(0), where the measured interplanar distance (0.22 nm) corresponded to the crystallographic {111} planes (Figures S9 and S11). EDX elemental mapping showed the presence of Rh and N homogeneously dispersed within silica surface (Figure 3). These results confirm the correct grafting of the ligands, and the homogeneous dispersion of RhNPs. Complementary, powder XRD analysis of RhNPs@SBA-15-Imz[NTf$_2$] (See ESI Figure S7) revealed an average crystal size of ca. 2.9 nm for Rh, as calculated using the Scherrer equation, which is consistent with values measured by HR-TEM. Although silica mesoporous structure was kept throughout functionalization, showing a type IV isotherms with H1 hysteresis loop in the N$_2$-adsorption-desorption isotherms (Figure 4 and S6), [61,53] a further decrease of surface area of RhNPs@SBA-15-Imz[NTf$_2$] was observed. Interestingly, although the material exhibited a type IV isotherm, the hysteresis loop was classified as type H2,[62] revealing more complex pore structures associated with blockage in a narrow range of pore necks and the pore mouth (aperture) of the original functionalized silica by the Rh nanoparticles.[53,61] Pore size distributions of the samples (inset, Figure 4) were estimated using the Barrett–Joyner–Halenda (BJH) method, revealing a pore distribution in the range of 2–5 nm.
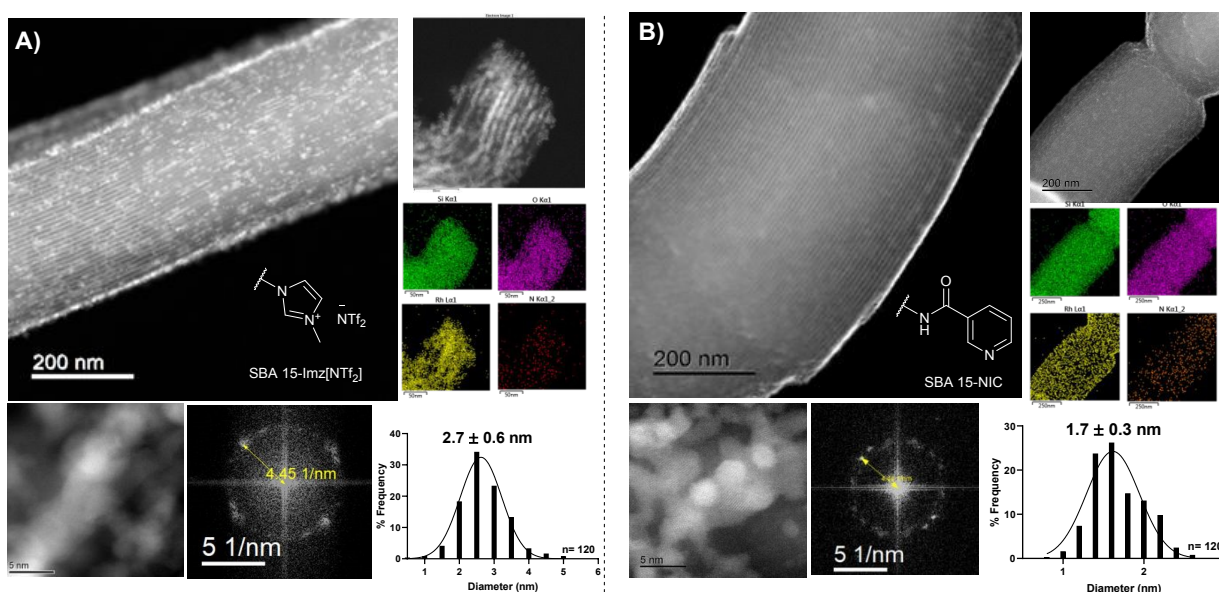
Figure 3. HAADF-STEM micrographs, along with corresponding FFT analysis, EDX elemental mapping, and size distribution histograms of RhNPs@SBA-15-Imz[NTf₂] (**A**) and RhNPs@SBA-15-NIC (**B**).
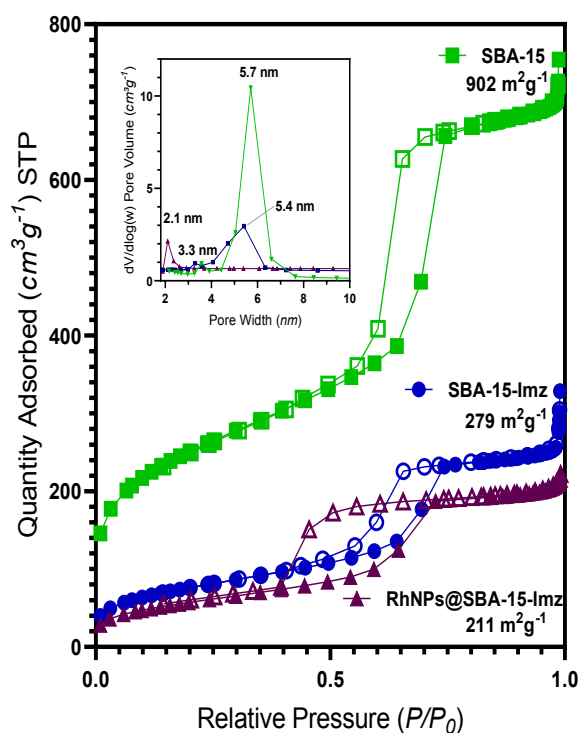
Figure 4. Adsorption–desorption N2 isotherms at 77 K of SBA-15 (green squares), SBA-15-Imz[NTf₂] (blue circles) and RhNPs@SBA-15-Imz[NTf₂] (purple triangles) and pore size distribution curves (inset, pore width were estimated by BJH model, cylindrical pores). Filled figures correspond to adsorption and hollow figures correspond to desorption.

X-ray photoelectron spectroscopy (XPS) survey spectrum confirmed the presence of nitrogen and rhodium (Figure S17 and S19). High-resolution spectrum of RhNPs@SBA-15-Imz[NTf₂] in the binding energy region corresponding to nitrogen (N 1s, Figure S18) exhibited three signals corresponding to imidazole nitrogen (401.3 eV), bistriflimide nitrogen (399 eV) and a nitrogen with lower binding energy possibly due to coordination to rhodium (397.8 eV). Binding energy region of rhodium (Rh 3d₃/₂ and Rh 3d₅/₂) showed a mixture of Rh(0) (307.4 eV), Rh(I) (308.5 eV) and Rh(III) (310.0 eV) (Figure 5). As shown, there is a high amount of Rh(0) in both materials. However, Imz[NTf₂] ligand exhibited a higher ability to prevent rhodium from oxidation, which is in agreement with the superior catalytic activity in hydrogenation reactions (*vide infra*).

Catalytic activity in hydrogenation reactions

To evaluate the potential for biomass substrate valorization, the starting reaction investigated was phenol (1) hydrogenation, chosen as a model substrate for molecules obtained from lignin.
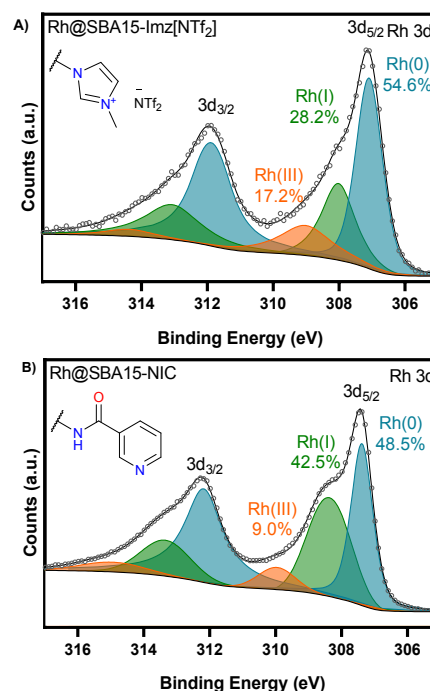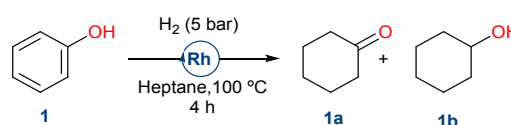

Figure 5. High-resolution XPS analysis in the binding region corresponding to rhodium. Rh 3d for RhNPs@SBA-15-Imz[NTf₂] (**A**) and RhNPs@SBA-15-NIC (**B**).

Phenol (1) was successfully hydrogenated under mild conditions (5 bar of H₂, 100 °C for 4 h) with moderate selectivity to cyclohexanone (1a) (Table 1). It must be noticed that such reduction was not possible using RhNPs supported on functionalized MCM-41, showing the importance of the silica-based support nature.[53] To further investigate the importance of mesostructured pores in silica, RhNPs supported on disordered microporous silica such as silica gel or non-porous silica like Stöber demonstrated low activity in the hydrogenation of phenol. Similarly, RhNPs supported on pristine SBA-15, which lacks nicotinamide functional groups and consequently suffers from poor RhNP stability, as previously reported,[53] showed no conversion or selectivity. Contrary to other reported catalysts, the ones presented herein favored the formation of the semi-hydrogenated ketone (1a) instead of the fully reduced cyclohexanol (1b).[63]

Taking advantage of the slow reduction to cyclohexanol (1b), we could prepare a tertiary amine in high yields by reductive amination. Utilizing reductive amination, substituted amines are synthesized from aldehydes or ketones along with less substituted amines.

Table 1. RhNPs catalytic hydrogenation of phenol

Journal Name

ARTICLE

Entry	Catalyst	Conv.%[a]	Yield 1a%[a]	Yield 1b%[a]	TON[b]
1	RhNPs@SBA-15-Imz[NTf₂]	>99	67	33	265
2	RhNPs@SBA-15-NIC	>99	73	27	289
3[c]	RhNPs@MCM-41-NIC	25	66	32	92
4	RhNPS@SiO₂-gel-NIC	3	70	29	8
5[d]	RhNPs@Stöber-NIC	<1	54	10	n.d
6[e]	RhNPs@SBA-15	10	77	15	31

Reaction conditions: 2 mmol of Phenol, 5 mg catalyst (0.25 mol% for RhNPs@SBA-15-Imz[NTf₂] and RhNPs@SBA-15-NIC; 0.18 mol% for RhNPs@ MCM-41-NIC), 2 mL of heptane, H₂ (5 bar), 100 °C, 4 h. [a] Determined by GC-FID. [b] TON = mmol of cyclohexanone x (mmol of Rh)[-1]. [c] From reference [53] [d] 35 % of benzene was detected. [e] 8% of benzene was detected.

This eco-friendly methodology prevents the need for reactive and potentially genotoxic reagents such as alkyl halides and sulphonates, commonly employed in conventional SN₂-type reactions of amines with alkylating agents. Furthermore, it mitigates concerns related to over-alkylation.[64] In this case the condensation between the formed ketone (1a) and morpholine, followed by hydrogenation of the enamine is presented (Scheme 3).[65-68]
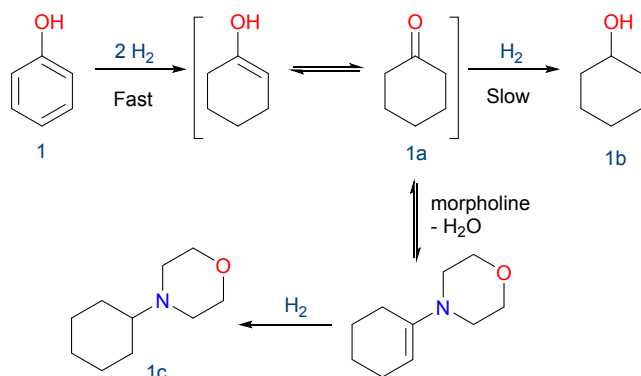
Scheme 3. RhNPs catalyzed reductive amination of phenol and morpholine.

Both catalysts yielded the corresponding 4-cyclohexylmorpholine (1c) with complete phenol conversion, high selectivity towards **1c**, and high turnover number (TON) (Table 2). As mentioned above, those materials had a superior activity compared to RhNPs supported on functionalized MCM-41.[53] Being slightly more active, RhNPS@SBA-15-Imz[NTf₂] was selected for recycling experiments and scope broadening of the reaction.

To evaluate the robustness and reusability of RhNPS@SBA-15-Imz[NTf₂], (Figure 6) we conducted the reductive amination of phenol (**1**) with morpholine, but also the reduction of cyclohexene as benchmark reactions. (ESI, Scheme 1) In the case of reductive amination of phenol and morpholine, no significant loss of activity nor selectivity were observed during the first 3 runs, with excellent yields of the desired product (Figure 6A).

Table 2. RhNPs catalyzed tandem reductive amination of phenol.

Entry	Catalyst	Conv.%[a]	Yield 1c%[a]	TON[b]
1	RhNPs@SBA-15-Imz[NTf₂]	>99	98	392
2	RhNPs@SBA-15-NIC	>99	97	384
3[c]	RhNPs@MCM-41-NIC	84	78	364

Reaction conditions: 2 mmol of Phenol, 2.5 mmol of morpholine, 5 mg catalyst (0.25 mol% for RhNPs@SBA-15-Imz[NTf₂] and RhNPs@SBA-15-NIC; 0.18 mol% for RhNPs@ MCM-41-NIC), 2 mL of heptane, H₂ (5 bar), 100 °C, 6 h. [a] Determined by GC-FID. [b] TON = mmol of products x (mmol of Rh)[-1]. [c] From reference [53]

Activity decreased on the 4th run, likely due to accumulation of morpholine on the catalyst surface, poisoning its activity. Nevertheless, a cumulative TON of 2633 could be achieved. On the contrary, cyclohexene (**2**) hydrogenation (ESI, Scheme 1) kept constant after 5 runs, showing that the catalyst is still active and certainly not poisoned, reaching a cumulative TON of 3976.

HAADF-STEM micrographs of the catalyst after catalytic reductive amination of phenol and morpholine reaction did not exhibit any sign of RhNPs agglomeration nor metal leaching. (Figure S16) Moreover, TEM images of spent catalyst still show {111} crystallographic planes for fcc Rh(0) and verify by FFT of RhNPs (ESI Figure S16). In addition, rhodium was not detected by MP-AES analyses of the organic phase after hydrogenation reaction, proving no metal leaching. These results highlight the important role of silica-supported *N*-stabilizers in the design for easy recycling applications and extending catalyst shelf-life.
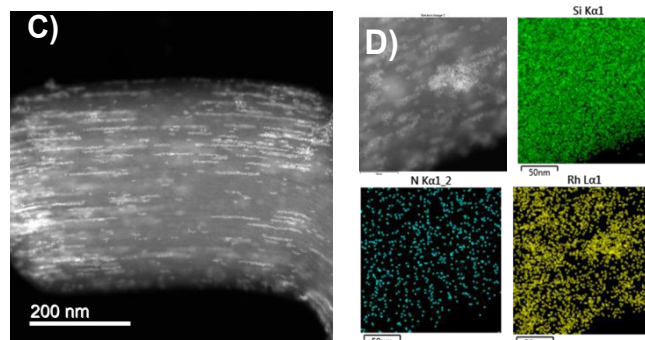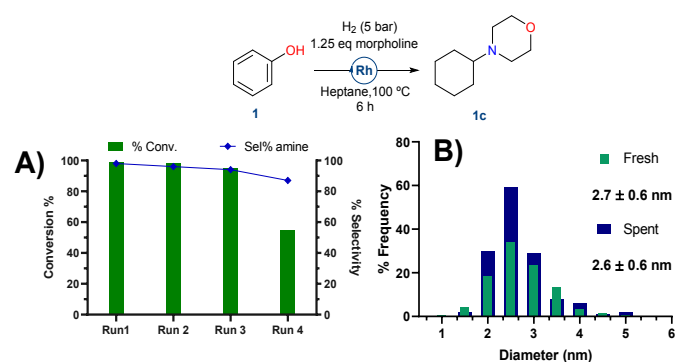
ARTICLE

Figure 6. (A) Recycling of RhNPs@SBA-15-Imz[NTf2] catalyst for the reductive amination of phenol; (B) RhNPs size distribution (E; n= 120 particles) of spent catalyst; (C) HAADF-STEM image (200 nm) and (D) EDX elemental mapping of spent RhNPs@SBA-15-Imz[NTf2],

Table 3. Collection of data from literature concerning to phenolics derivatives reductive amination catalyzed by metal nanoparticles.

Entry	MNPs	Support	p H$_2$ (bar)	Amine eq.	Temp. (°C)	Time (h)	Metal amount (mol %)	Solvent	Conv. %	Yield %	TON[a]	TOF[b] (h^{-1})	Ref.
1			None [c]	2.0	60	6	9.00	H$_2$O	100	96	11	1.8	66
2			None [d]	1.2	120	24	7.00	Toluene	----	90	13	0.5	69
3		C	20	2.5	140	24	6.00	m-xylene	99	99	17	0.7	68
4	Pd		10	1.5	90	6	3.00	m-xylene	>99	>99	33	5.5	67
5			5	1.1	100	15	2.00	H$_2$O	-----	85	43	2.9	70
6			1	1.0	60	6	2.00	p-xylene	----	84	43	7.2	71
7		Al$_2$O$_3$	1	2.0	70	10	9.30	Hexane	95	94	11	1.1	72
8	Ni		8	1.4	160	3	10.00	Toluene	99	99	10	3.3	73
9		C	1.5	1.4	120	20	2.10	t-amyl alcohol	>99	64	65	3.3	74
10	Rh	PVP	5	1.4	40	24	2.00	H$_2$O	>99	96	48	2	75
11		SBA-15-Imz[NTf$_2$]	5	1.25	100	6	**0.25**	Heptane	>99	98	**392**	65	This work
12		SBA-15-NIC	5	1.25	100	6	**0.25**	Heptane	>99	97	**384**	64	

[a] Data found in corresponding reference TON= mmol of amine x mmol metal $^{-1}$,[b] TOF= TON x h^{-1}; [c] HCOONa (20 equiv.) used as reductant; [d] HCOONa (6 equiv.)

Comparing the results obtained in this work with those found in the literature (Table 3), we observed a superior activity of Rh nanoparticles in terms of TON (Table 3, entries 9-12). This can be attributed to their high rhodium's π-acidity,[76,77] allowing strong interactions of aromatic rings, which facilitate efficient hydrogenation processes. The integration of RhNPs into molecularly modified silica matrices further enhances their catalytic performance by providing a robust and high-surface-area support that stabilizes the nanoparticles and optimizes their dispersion. This setup ensures that the catalytic sites remain highly accessible, leading to improved turnover numbers (almost 6 times higher) and turnover frequencies (TOF, 20 times higher), as evidenced by experimental data (Table 3, entries 11-12) showing substantial increases in conversion and yield percentages. Moreover, the tailored surface chemistry of imidazolium and nicotinamide moieties allows for precise interaction with complex biomass-derived molecules, thereby enhancing selectivity and reducing undesired side reactions.

With this catalyst in hand, we broadened the reaction scope of alkene derivatives (see Figure 7) as well as other functional groups (Figures 8 and 9). Styrene (**3**) and a range of biomass-derived alkenes, such as limonene (**4**), α-pinene (**5**), safrole (**6**), estragole (**7**), and eugenol (**8**), underwent facile hydrogenation under mild conditions and low metal loadings (see Figure 7, conditions A: heptane, 5 bar H$_2$, 3 h). However, terpene derivatives like geraniol (**9**), a primary component of rose essential oil, and myrcene (**10**), found in parsley essential oil, needed harsher conditions to achieve complete hydrogenation (conditions B: heptane, 20 bar H$_2$, 8 h). Remarkably, under

solventless conditions, the double bond of oleic acid (**11**) and squalene (**12**) were efficiently hydrogenated to yield very high conversion rates, demonstrating the robustness of RhNPs@SBA-15-Imz[NTf$_2$].
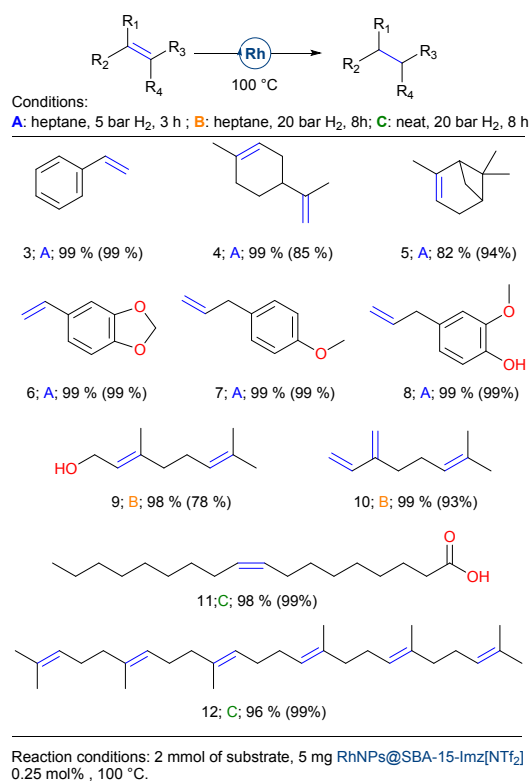

Reaction conditions: 2 mmol of substrate, 5 mg RhNPs@SBA-15-Imz[NTf$_2$] 0.25 mol% , 100 °C.

Figure 7. RhNPs catalysed hydrogenation of biomass-derived alkenes

Other functional groups could also be hydrogenated with this catalytic system, including nitriles, nitro compounds, aromatics, and quinoline (Figure 8). Benzonitrile (**13**) was reduced to benzylamine under standard conditions (20 bar H_2, 2 h) in the presence of 2 equivalents of ammonium hydroxide. As previously reported, the addition of aqueous ammonia prevents the formation of dibenzylamine and drives the reaction to benzylamine selectively.[78,79] Nitrobenzene (**14**) was hydrogenated to yield aniline (**14a**) under high hydrogen pressure (40 bar H_2) while no traces of cyclohexylamine were detected during nitrobenzene hydrogenation. Interestingly, aromatics bearing electron-donor groups could also be reduced under these harsher conditions. Indeed, toluene (**15**) gave methylcyclohexane (**15a**) in high yields as well as quinoline (**16**) gave 1,2,3,4-tetrahydroquinoline (**16a**). Levulinic acid (**17**), being a molecule potentially obtained from starch of lignocellulose, was hydrogenated in moderate yield but with excellent selectivity to γ-valerolactone (**17a**), used as solvent or in perfume industry.[80]
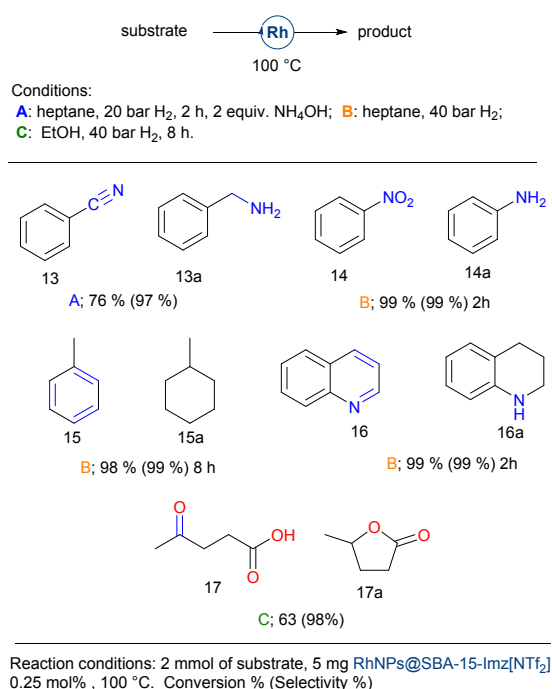

Conditions:
A: heptane, 20 bar H_2, 2 h, 2 equiv. NH_4OH; **B**: heptane, 40 bar H_2;
C: EtOH, 40 bar H_2, 8 h.

A; 76 % (97 %)

B; 99 % (99 %) 2h

B; 98 % (99 %) 8 h

B; 99 % (99 %) 2h

C; 63 (98%)

Reaction conditions: 2 mmol of substrate, 5 mg RhNPs@SBA-15-Imz[NTf₂]
0.25 mol% , 100 °C. Conversion % (Selectivity %)
Figure 8. RhNPs catalyzed hydrogenation of different functional groups

Finally, we evaluate the hydrogenation of biomass-derived aldehydes (Figure 9).

Furfural (**18**) is one of the most promising biomass-derived platform molecules, with great potential to produce fuel additives and high-value chemicals. Among its various transformations, the catalytic hydrogenation of furfural into furfuryl alcohol stands out as a crucial process in the chemical conversion of bio-derived compounds.[81] In pursuit of environmentally sustainable alternatives, supported noble and transition-metal catalysts, including Pt,[82] Ir,[83] Pd,[84] Ru,[85] Ni,[86] Co,[87] Rh,[88] and other bimetallic systems have been explored. These catalysts offer the potential to selectively hydrogenate the carbonyl group while preserving the carbon-carbon double bonds. However, many of these catalysts require elevated temperatures, and/or the use of acid additives, which can be limiting factors for their practical application.

Using the catalytic system presented herein, neat furfural (1 mmol) (**18**) could be hydrogenated, but only moderate yields were achieved. Although benzaldehyde (**19**) could be reduced in high yield, vanillin (**20**) affords the corresponding alcohol in moderate yield, and anisaldehyde (**21**) and syringaldehyde (**22**) gave both very poor results. It seems that electron-donor groups deactivate the carbonyl moiety, preventing its hydrogenation.
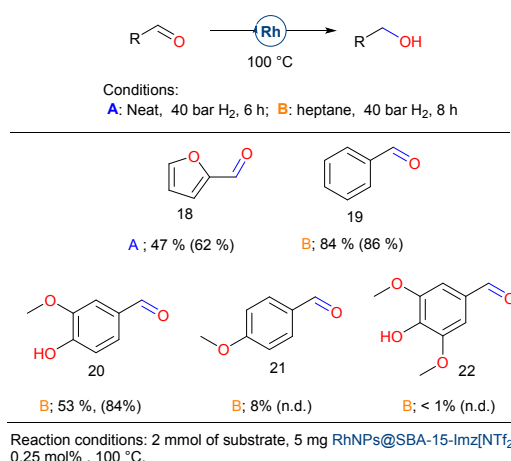

Conditions:
A: Neat, 40 bar H_2, 6 h; **B**: heptane, 40 bar H_2, 8 h

A ; 47 % (62 %)

B; 84 % (86 %)

B; 53 %, (84%)

B; 8% (n.d.)

B; < 1% (n.d.)

Reaction conditions: 2 mmol of substrate, 5 mg RhNPs@SBA-15-Imz[NTf₂]
0.25 mol% , 100 °C.
Figure 9. RhNPs catalyzed hydrogenation of biomass-derived aldehydes

The two catalytic materials studied herein differ in the nature of their stabilization, leading to distinct activities towards the hydrogenation of furfural (Figure 10). RhNPs@SBA-15-Imz[NTf2] achieved a TON of approximately 579, whereas RhNPs@SBA-15-NIC only reached a TON of 289. The neutral and ionic nature of the silica grafting fragments showed a different role as stabilizers affecting the morphology and size of RhNPs as shown in the characterization section. In addition, Supported Ionic Liquid Phases (SILPs) are able to modulate the chemical environment around active sites, controlling reaction selectivity in various cases.[89] In our study, the covalently supported imidazolium bistriflimide forms a thin IL layer, which upon RhNPs formation, limits the interaction of Rh with silanol groups (Si-OH). High-resolution O 1s XPS spectra (Figure 10-E) reveal that only 6% of Rh-O species (529.95 eV)[90] are present, resulting in more favorable interactions with furfural and thus higher TONs. In contrast, the neutral nicotinamide fragment supported on silica does not form this thin layer, leading to greater metal-silanol interactions (17% Rh-O by XPS, Figure 10-D) that block the RhNPs surface, thereby decreasing the TONs. This highlights the critical role of stabilizer choice in optimizing catalytic performance.
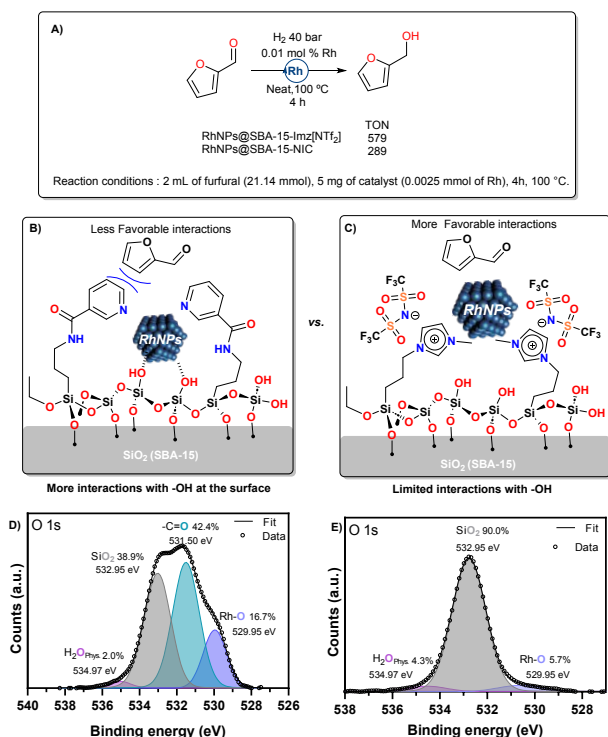
ARTICLE

Figure 10. A) RhNPs performance on Furfural hydrogenation in neat conditions; Proposed interactions of RhNPs with B) SBA-15-NIC and C) SBA-15-Imz[NTf$_2$] supports; High resolution XPS spectra of D) RhNps@SBA-15-NIC and E) RhNPs@SBA-15-Imz[NTf$_2$].

Conclusions

Overall, we synthesized RhNPs supported on *N*-functionalized silica-based materials. Specifically, we chose SBA-15 as the support and functionalized it with nicotinamide or imidazolium-based ionic liquid. Solid-state ^{29}Si and ^{13}C NMR experiments confirmed the successful anchoring of the ligands to the silica surface. RhNPs@SBA-15-Imz[NTf$_2$] and RhNPs@SBA-15-NIC were easily prepared through organometallic precursor decomposition and thoroughly characterized. These materials exhibited small, spherical, and well-dispersed fcc Rh nanoparticles located on the support surface. XPS analyses revealed the presence of metallic rhodium, along with Rh(I) and Rh(III) species.

We then evaluated the catalytic performance of these materials in the hydrogenation of various functional groups, including alkenes, aldehydes, nitriles, ketones, nitro compounds, quinolines, and aromatic rings. Our particular focus was on the hydrogenation of biomass-derived substrates such as limonene, safrole, geraniol, levulinc acid, and furfural. Notably, the catalyst exhibited excellent recyclability, maintaining its activity, and preventing metal leaching over multiple cycles.

In general, reactions involving excess amine poison the catalyst activity, preventing the reuse of the material.

Finally, the nature of the stabilization in RhNPs catalysts significantly influences their activity towards furfural hydrogenation. RhNPs@SBA-15-Imz[NTf$_2$], with its ionic imidazolium bistriflimide stabilizer limits silanol interactions with RhNPs, resulting in active systems for the hydrogenation of

furfural. In contrast, RhNPs@SBA-15-NIC, with its neutral nicotinamide stabilizer showed Rh-silanol interactions, blocking the RhNPs surface and decreasing its catalytic activity. This highlights the critical role of stabilizer choice in optimizing catalytic performance.

Experimental section

General

Unless otherwise indicated, all manipulations and procedures were performed under nitrogen atmosphere (99.998%) using standard Schlenk techniques. Organic solvents were distilled from appropriate desiccant under a nitrogen atmosphere and stored over activated 3 Å molecular sieves all reagents were acquired from commercial suppliers and used as received. Micro analysis of the synthesized materials was carried out at USAII ("Unidad de Servicios de Apoyo a la Investigación y a la Industria" of Faculty of Chemistry, UNAM). Infrared spectra were recorded on a Perkin-Elmer FTIR/ FIR Spectrum 400 spectrometer. NMR spectra ^1H, {^1H} COSY (Correlation Spectroscopy), ^{13}C{^1H} were recorded on a JEOL ECZ600R spectrometer at 14.09 T (600 MHz for ^1H), chemical shifts (δ, ppm) were calibrated relative to the residual solvent peak. Elemental analysis was acquired on a Perkin-Elmer 2400 Elemental Analyzer for CHNS using cysteine as the calibration compound. Thermogravimetric (TGA) data were recorded on a Perkin-Elmer TGA 4000 analyser from room temperature to 900 °C with a speed of 5 °C/min. For surface area analysis a Micromeritics TriStar 3000 Surface Area and Pore Size Analyzer was used to produce nitrogen physisorption isotherms at 77 K on synthesized materials, the data were fit using a Brunauer-Emmett-Teller (BET) model to determine the apparent surface areas of the materials. The average pore diameter and cumulative pore volumes were calculated using the Barrett-Joyner-Halenda (BJH) model for mesopores. Samples were degassed under vacuum at 130 °C for 18 h prior to the analysis. Scanning electron microscope (SEM) micrographs of synthesized materials were obtained on a JEOL JSM-5900-LV microscope. Particle diameter was determined counting at least 100 individual particles with the software package Digimizer 4.6.1.[91] Transmission electron microscopy (TEM) images of synthesized materials before and after recycling were obtained on a JEOL ARM200F microscope operating at an accelerating voltage of 200 kV. Nanoparticle measurements were performed with the software package DigitalMicrograph 3.30.2017.0.[93] XRD patterns were recorded on an X-ray powder diffractometer Bruker AXS model D8 advance Davinci (Theta-Theta configuration) equipped with Lynxeye detector. The average MNP crystallite size was calculated from the full width at half maximum (FWHM) of the peaks using the Scherrer equation (1), where τ is the average crystallite size, K is a constant with a value of 0.9, λ is the X-ray wavelength, β is the FWHM in radians, and θ is the diffraction angle.

$$\tau = \frac{K\lambda}{\beta Cos(\theta)} \qquad (1)$$

ARTICLE

XPS measurements were performed using a Thermo Scientific K-Alpha spectrometer, with MAGCIS ion source for depth profiling analysis and surface cleaning. The assignment of chemical components of core level Rh 3d was made by comparison to the referenced values reported in the literature.[53,93-95] Synthesis of supported rhodium nanoparticles was carried out in a 100 mL Fisher-Porter vessel. Catalytic reactions were performed in a Parr Multi Reactor 500 system. Catalytic conversions were determined on a Varian 3800 gas chromatograph with a capillary column DB-WAX (30 m × 0.32 mm × 0.25 mm) coupled to an FID detector, using internal standard method.

Solid-state NMR experiments were recorded at the LCC (Toulouse) on a Bruker Avance 400 spectrometer equipped with 2.5, 3.2- or 4-mm probes. Samples were packed into 4 mm zirconia rotors. The rotors were spun at 8 kHz at 293 K. ^{13}C CP-MAS and ^{29}Si UDEFT-MAS spectra were recorded with a recycle delay of 2 s and contact times of 3 ms and 4 ms, respectively, spectra deconvolution was fitted using the DMfit software.[96] Precursor methoxy(1,5-cyclooctadiene)rhodium(I) dimer [Rh(μ-OMe)(1,5-COD)]$_2$,[97] N-(3-(triethoxysilyl)propyl) nicotinamide, (NIC),[53,98] 1-methyl-3-(3-(triethoxysilyl)propyl)-1H-imidazolium chloride,[99] were prepared following previously reported method.

SBA-15 was obtained according to Zhao et. al.,[100] The polymeric template was removed by calcination at 550 °C in air for 5 h, and the resulting synthesized rod-shaped mesoporous silica was denoted as SBA-15.

General synthesis of functionalized mesoporous silica SBA-15

In a Schlenk flask, SBA-15 (3 g) was dried at 80 °C for 24 h prior use. Then SBA-15 was suspended by sonication in dry toluene (140 mL) under nitrogen for 15 min, then the mixture was treated with the corresponding silane (9.2 to 9.3 mmol, 100 Wt.% vs SiO$_2$). The mixture was stirred at reflux temperature (120 °C) for 72 h. The solid was recovered by filtration, washed five times with hot toluene and ethanol. The resulting white solid dried under reduced pressure for 12 h.

SBA-15-Imz[NTf$_2$]

Additional to the above procedure the material SBA-15-Imz[Cl] were further treated with LiNTf$_2$ for salt metathesis. Briefly, under nitrogen, the solid obtained SBA-15-Imz[Cl] was resuspended in dry dichloromethane and treated with an excess of bis(trifluoromethane)sulfonimide lithium salt (1.5 g, 5.2 mmol). The mixture was stirred at room temperature (ca. 25 °C) for 72 h. The solid was separated by filtration and washed five times with hot dry ethanol. The obtained solid was dried under reduced pressure for 12 h.

FT-IR(ATR) ν (cm^{-1}): 3300 (ν SiO-H), 2900-2800 (ν C-H), 1574 (ν C=N imz), 1345 (ν S=O), 1184 (ν C-F), 1034 (ν Si-O-Si), 444 (ν Si-O). TGA: 32.9% Wt. organic content. **Elem. Anal. found** C, 11.71; H, 2.08; N, 3.75; S, 2.63. ^{13}C {^{1}H} CP-MAS (100 MHz, ppm): 135.71 (N-CH-N, Imz), 122.16 (N-CH-CH-N, Imz), 117.80(-CF$_3$, NTf$_2$), 58.16 (SiO-CH$_2$-CH$_3$), 50.80(N-CH$_2$-), 35.12 (-N-CH$_3$), 22.91 (Si-CH$_2$-CH$_2$-CH$_2$-N), 14.85 (SiO-CH$_2$-CH$_3$), 8.27 (-CH$_2$-Si-). **^{29}Si**

UDEFT-MAS (79 MHz, ppm) δ: -58.80 (T^2), -68.57 (T^3), -92.41 (Q^2), -101.68 (Q^3), -109.58 (Q^4).

SBA-15-NIC

FT-IR(ATR) ν (cm^{-1}): 3300 (ν SiO-H), 2900-2800 (ν C-H), 1646 (ν C=O), 1545 (δ N-H), 1060 (ν Si-O-Si), 705 (γ N-H), 440 (ν Si-O). **TGA**: 25.11% Wt. organic content. **Elem. Anal. found** C, 13.44; H, 2.25; N, 4.35. ^{13}C {^{1}H} CP-MAS (100 MHz, ppm): 163.44 (-C=O), 147.78 (-CH-, Py), 144.05 (-CH-, Py), 136.6 (-CH-, Py), 128.41 (C ipso, Py), 124.20 (-CH-, Py), 57.52 (SiO-CH$_2$-CH$_3$), 41.87 (-HN-CH$_2$-), 20.93 (CH$_2$-CH$_2$-CH$_2$), 16.09 (SiO-CH$_2$-CH$_3$), 9.45(-CH$_2$-Si-). **^{29}Si UDEFT-MAS** (79 MHz, ppm) δ: -59.10 (T^2), -67.54 (T^3), -92.59 (Q^2), -101.68 (Q^3), -109.61 (Q^4).

General synthesis of supported RhNPs on functionalized silicas

In a Fisher-Porter reactor, [Rh(μ-OMe)(1,5-COD)]$_2$ (105.9 mg, 0.219 mmol) and 405 mg of functionalized silica (SBA-15-NIC or SBA-15-Imz[NTf$_2$]) were suspended in dry THF (50 mL) under nitrogen atmosphere. This mixture was sonicated for five minutes to obtain a homogeneous pale-yellow suspension. The reactor was then charged with 3 bar of H$_2$ at room temperature and allowed to stir for 18 h. After the reaction time, the reactor was depressurized, and all volatiles were removed under reduced pressure to afford a black solid. The supported RhNPs (black solid) obtained, was dried under vacuum at 80 °C for 24 h.

General procedure for catalytic hydrogenation reactions

5 mg of RhNPs@SBA-15-Imz[NTf$_2$] or RhNPs@SBA-15-NIC were added to a 25 mL stainless steel reactor flask equipped with glass liner and a stirring magnet, together with solvent (2 mL), and substrate(s) (2 mmol). The Reaction mixture was then pressurized with hydrogen (5, 20 or 40 bar) and stirred (300 rpm) at 100 °C for the specified time. After the reaction was completed, the reactor vessel was cooled with an ice bath and slowly depressurized. The crude reaction was filtered through a Celite® pad prior to being analysed by GC. For acidic substrates i.e. levulinic acid or oleic acid, a 100 mL Hastelloy® reactor with glass liner was employed.

Author Contributions

I.T.P.D.: investigation, formal analysis, methodology, and visualization; D.M.: investigation, formal analysis, and methodology; K.P.S.M.: formal analysis, and methodology; B.P.M.: data curation; D.A.: writing – review & editing; A.R.: project administration, supervision, visualization, and writing – original draft; I.G.R.: conceptualization, funding acquisition, project administration, supervision, visualization, resources, and writing – review & editing.

Conflicts of interest

The authors declare no competing financial interest.

Acknowledgements

Notes and references

1 Ragauskas, A. J.; Williams, C.K.; Davison, B. H.; Britovsek, G.; Cairney, J.; Eckert, C. A.; Frederick, W. J.; Hallett, J. P.; Leak, D. J.; Liotta, C. L.; Mielenz, J. R.; Murphy, R.; Templer, R.; Tschaplinski, T. The Path Forward for Biofuels and Biomaterials *Science*, **2006**, *311*, 484–489. https://doi.org/10.1126/science.1114736

2 Huber, G. W.; Iborra, S.; Corma, A. Synthesis of Transportation Fuels from Biomass: Chemistry, Catalysts, and Engineering. *Chem. Rev.*, **2006**, *106*, 4044–4098. https://doi.org/10.1021/cr068360d

3 Corma, A.; Iborra, S.; Velty, A. Chemical Routes for the Transformation of Biomass into Chemicals. *Chem. Rev.*, **2007**, *107*, 2411–2502. https://doi.org/10.1021/cr050989d

4 Colmenares, J. C.; Varma, R. S.; Nair, V. Selective photocatalysis of lignin-inspired chemicals by integrating hybrid nanocatalysis in microfluidic reactors. *Chem. Soc. Rev.*, **2017**, *46*, 6675–6686. https://doi.org/10.1039/C7CS00257B

5 Li, C.; Zhao, X.; Wang, A.; Huber, G. W.; Zhang, T. Catalytic Transformation of Lignin for the Production of Chemicals and Fuels. *Chem. Rev.*, **2015**, *115*, 11559–11624. https://doi.org/10.1021/acs.chemrev.5b00155

6 Jing, Y.; Dong, L.; Guo, Y.; Liu, X.; Wang, Y. Chemicals from Lignin: A Review of Catalytic Conversion Involving Hydrogen. *ChemSusChem*, **2020**, *13*, 4181-4198. https://doi.org/10.1002/cssc.201903174

7 Xu, C.P.; Arancon, R. A. D.; Labidi, J.; Luque, R. Lignin depolymerisation strategies: towards valuable chemicals and fuels. *Chem. Soc. Rev.*, **2014**, *43*, 7485–7500. https://doi.org/10.1039/C4CS00235K

8 Shuai, L.; Amiri, M. T.; Questell-Santiago, Y. M.; Héroguel, F.; Li, Y.; Kim, H.; Meilan, R.; Chapple, C.; Ralph, J.; Luterbacher, J. S. Formaldehyde stabilization facilitates lignin monomer production during biomass depolymerization. *Science*, **2016**, *354*, 329–333. https://doi.org/10.1126/science.aaf7810

9 Wu, X.; Fan, X.; Xie, S.; Lin, J.; Cheng, J.; Zhang, Q.; Chen, L.; Wang, Y. Solar energy-driven lignin-first approach to full utilization of lignocellulosic biomass under mild conditions. *Nat. Catal.*, **2018**, *1*, 772–780. https://doi.org/10.1038/s41929-018-0148-8

10 Nakagawa, Y.; Tomishige, K. Production of 1,5-pentanediol from biomass via furfural and tetrahydrofurfuryl alcohol. *Catal. Today*, **2012**, *195(1)*, 136-143. https://doi.org/10.1016/j.cattod.2012.04.048

11 Production of Biofuel via Hydrogenation of Lignin from Biomass in New Advances in Hydrogenation Processes: Fundamental and Applications (Ed: Ravanchi, M. T.). Abdullah, B.; Muhammad, S. A. F. A. S.; Nik Mahmood, N. A. *IntechOpen* **2017**, 289-305. http://dx.doi.org/10.5772/66108

12 Jin, X.; Fang, T.; Wang, J.; Liu, M.; Pan, S.; Subramaniam, B.; Shen, J.; Yang, C.; Chaudhari, R. V. Nanostructured Metal Catalysts for Selective Hydrogenation and Oxidation of Cellulosic Biomass to Chemicals. *Chem. Rec.*, **2019**, *19(9)*, 1952-1994. https://doi.org/10.1002/tcr.201800144

13 Tomishige, K.; Nakagawa, N.; Tamura, M. Selective hydrogenolysis and hydrogenation using metal catalysts directly modified with metal oxide species. *Green Chem.*, **2017**, *19*, 2876-2924. https://doi.org/10.1039/C7GC00620A

14 Racha, A.; Samanta, C.; Sreekantan, S.; Marimuthu, B. Review on Catalytic Hydrogenation of Biomass-Derived Furfural to Furfuryl Alcohol: Recent Advances and Future Trends. *Energy Fuels*, **2023**, *37(16)*, 11475-11496. https://doi.org/10.1021/acs.energyfuels.3c01174

15 Schlaf, M. Selective deoxygenation of sugar polyols to a,w-diols and other oxygen content reduced materials—a new challenge to homogeneous ionic hydrogenation and hydrogenolysis catalysis. *Dalton Trans.*, **2006**, 4645-4653. https://doi.org/10.1039/B608007C

16 Bordet, A.; Moos, G.; Welsh, C.; Licence, P.; Luska, K. L.; Leitner, W. Molecular Control of the Catalytic Properties of RhodiumNanoparticles in Supported Ionic Liquid Phase (SILP) Systems. *ACS Catal.*, **2020**, *10*, 13904-13912. https://doi.org/10.1021/acscatal.0c03559

17 Zhang, Y.; Li, A.; Kubu, M.; Shamzhy, M.; Cejka, J. Highly selective reduction of biomass-derived furfural by tailoring the microenvironment of Rh@BEA catalysts. *Catal. Today*, **2022**, *390-391*, 295-305. https://doi.org/10.1016/j.cattod.2021.09.031

18 Liu, S.; Govindarajan, N.; Chan, K. Understanding Activity Trends in Furfural Hydrogenation on Transition Metal Surfaces. *ACS Catal.*, **2022**, *12(20)*, 12902-12910. https://doi.org/10.1021/acscatal.2c03822

19 Lee, J.; Xu, Y.; Huber, G. W. High-throughput screening of monometallic catalysts for aqueous-phase hydrogenation of biomass-derived oxygenates. *Appl. Catal. B: Environ.*, **2013**, *140-141*, 98-107. https://doi.org/10.1016/j.apcatb.2013.03.031

20 Balakrishanan, M.; Sacia, E. R.; Bell, A. T. Selective Hydrogenation of Furan-Containing Condensation Products as a Source of Biomass-Derived Diesel Additives. *ChemSusChem*, **2014**, *7(10)*, 2796-2800. https://doi.org/10.1002/cssc.201402764

21 Luo, Y.; Yi, J.; Tong, D.; Hu, C. Production of γ-valerolactone via selective catalytic conversion of hemicellulose in pubescens without addition of external hydrogen. *Green Chem.*, **2016**, *18*, 848-857. https://doi.org/10.1039/C5GC01775K

22 Li, M.; Li, G.; Li, N.; Wang, A.; Dong, W.; Wang, X.; Cong, Y. Aqueous phase hydrogenation of levulinic acid to 1,4-pentanediol. *Chem. Commun.*, **2014**, *50*, 1414-1416. https://doi.org/10.1039/C3CC48236G

23 Ban, C.; Jeon, W.; Woo, H. C.; Kim, D. H. Catalytic Hydrogenation of Macroalgae-Derived Alginic Acid into Sugar Alcohols. *ChemSusChem*, **2017**, *10(24)*, 4891-4898. https://doi.org/10.1002/cssc.201701860

24 Duan, Y.; Zhang, C.; Deng, D.; Sui, D.; Gao, X.; Yang, Y. Hydrogenation of BHMF with controllable selectivity to tetrahydropyranone and 1-hydroxy-2,5-hexanedione under atmospheric H2 pressure. *Green Chem.*, **2023**, *25*, 1823-1834. https://doi.org/10.1039/D2GC04637G

25 Vono, L. L. R.; Broicher, C.; Philippot, K.; Rossi, L. M. Tuning the selectivity of phenol hydrogenation using Pd, Rh and Ru nanoparticles supported on ceria- and titania-modified silicas. *Catal. Today*, **2021**, *381*, 126-132. https://doi.org/10.1016/j.cattod.2020.07.078

Nanoscale Accepted Manuscript

26 Song, Y.; Gutiérrez, O. Y.; Herranz, J.; Lercher, J. A. Aqueous phase electrocatalysis and thermal catalysis for the hydrogenation of phenol at mild conditions. *Appl. Catal. B: Environ.*, **2016**, *182*, 236-246. https://doi.org/10.1016/j.apcatb.2015.09.027

27 Yu, C.; Wu, W.; Gao, M.; Liu, Y. Modified Cellulose with BINAP-Supported Rh as an Efficient Heterogeneous Catalyst for Asymmetric Hydrogenation. *Catalysts*, **2022**, *12*, 83. https://doi.org/10.3390/catal12010083

28 Vandekerkhove, A.; Claes, L.; De Shouwer, F.; Van Goethem, C.; Vankelecom, I. F. J.; Lagrain, B.; De Vos, D. E. Rh-Catalyzed Hydrogenation of Amino Acids to Biobased Amino Alcohols: Tackling Challenging Substrates and Application to Protein Hydrolysates. *ACS Sustainable. Chem. Eng.*, **2018**, *6(7)*, 9218-9228. https://doi.org/10.1021/acssuschemeng.8b01546

29 Toth, I.; Tukacs, J. M.; Mika, L. T. Kinetic and Mechanistic Studies of the Selective Hydrogenation of (E)-Chalcones in Biomass-Derived γ-Valerolactone Catalyzed by Rh–PPh3 Complexes. *ChemCatChem*, **2023**, *15(7)*, e202201480. https://doi.org/10.1002/cctc.202201480

30 Zou, G.; Zhong, W.; Mao, L.; Xu, Q.; Xiao, J.; Yin, D.; Xiao, Z.; Kirk, S. R.; Shu, T. A non-nitric acid method of adipic acid synthesis: organic solvent- and promoter-free oxidation of cyclohexanone with oxygen over hollow-structured Mn/TS-1 catalysts, *Green Chem.*, **2015**, *17*, 1884–1892. https://doi.org/10.1039/C4GC02333A

31 Etayo, P.; Vidal-Ferran, A. Rhodium-catalysed asymmetric hydrogenation as a valuable synthetic tool for the preparation of chiral drugs. *Chem. Soc. Rev.*, **2013**, *42*, 728-754. https://doi.org/10.1039/C2CS35410A

32 Murphy, S. K.; Park, J.-W.; Cruz, F. A.; Dong, V. M. Rh-catalyzed C–C bond cleavage by transfer hydroformylation. *Science*, **2015**, *347*, 56-60. https://doi.org/10.1126/science.1261232

33 Rhodium Catalysed hydroformylation, (Eds: P. W. N. M. Van Leeuwen, C. Claver), Kluwer Academic Publishers, New York, 2002.

34 Pérez-Alonso, A.; Minh, D. P.; Pla, D.; Gómez, M. A Cooperative Rh/Co-Catalyzed Hydroaminomethylation Reaction for the Synthesis of Terpene Amines. *ChemCatChem*, **2023**, *15(13)*, e202300501. https://doi.org/10.1002/cctc.202300501

35 Dupont, J.; Scholtten, J. D. On the structural and surface properties of transition-metal nanoparticles in ionic liquids. *Chem. Soc. Rev.*, **2010**, *39*, 1780-1804. https://doi.org/10.1039/B822551F

36 Serrano-Maldonado, A.; Reina, A.; Portales-Martínez, B.; Guerrero-Ríos, I. Thioglycerol-Stabilized Rhodium Nanoparticles in Biphasic Medium as Catalysts in Multistep Reactions. *Eur. J. Inorg. Chem.*, **2020**, *26*, 2506-2511. https://doi.org/10.1002/ejic.202000451

37 Serrano-Maldonado, A.; Dang-Bao, T.; Favier, I.; Guerrero-Ríos, I.; Pla, D.; Gómez, M. Glycerol Boosted Rh-Catalyzed Hydroaminomethylation Reaction: A Mechanistic Insight. *Chem. Eur. J.*, **2020**, *26*, 12553-12559. https://doi.org/10.1002/chem.202001978

38 Ndolomingo, M. J.; Ndzondelelo, B.; Meijboom, R. Review of supported metal nanoparticles: synthesis methodologies, advantages and application as catalysts. *J. Mater. Sci.*, **2020**, *55*, 6195-6241. https://doi.org/10.1007/s10853-020-04415-x

39 Ganji, S.; Enumula, S. S.; Marella, R. K.; Rao, K. S. R.; Burri, D. R. RhNPs/SBA-NH2: a high-performance catalyst for aqueous phase reduction of nitroarenes to aminoarenes at room temperature. *Catal. Sci. Technol.*, **2014**, *4*, 1813-1819. https://doi.org/10.1039/C4CY00143E

40 Vunain, E.; Ncube, P.; Jalama, K.; Meijboom, R. Confinement effect of rhodium(I) complex species on mesoporous MCM-41 and SBA-15: effect of pore size on the hydroformylation of 1-octene. *J. Porous Mater.*, **2018**, *25*, 303-320. https://doi.org/10.1007/s10934-017-0443-9

41 Choi, I.; Chun, S.; Chung, Y. K. Bimetallic Cobalt–Rhodium Nanoparticle-Catalyzed Reductive Amination of Aldehydes with Nitroarenes Under Atmospheric Hydrogen. *J. Org. Chem.*, **2017**, *82*, 12771-12777. https://doi.org/10.1021/acs.joc.7b02019

42 Huang, L.; Wang, Z.; Geng, L.; Chen, R.; Xing, W.; Wang, Y.; Huang, J. Selective and recyclable rhodium nanocatalysts for the reductive N-alkylation of nitrobenzenes and amines with aldehydes *RSC Adv.*, **2015**, *5*, 56936-56941. https://doi.org/10.1039/C5RA05243B

43 Muñoz, M.; de Pedro, Z. M.; Casas, J. A.; Rodríguez, J. J. Improved γ-alumina-supported Pd and Rh catalysts for hydrodechlorination of chlorophenols. *Appl, Catal. A: Gen.*, **2014**, *488*, 78-85. https://doi.org/10.1016/j.apcata.2014.09.035

44 Sharma, S.; Bhattacherjee, D.; Das, P. Supported Rhodium Nanoparticles Catalyzed Reduction of Nitroarenes, Arylcarbonyls and Aryl/Benzyl Sulfoxides using Ethanol/Methanol as In Situ Hydrogen Source. *Adv. Synth. Catal.*, **2018**, *360(11)*, 2131-2137. https://doi.org/10.1002/adsc.201701609

45 Pal, N.; Bhaumik, A.; Mesoporous materials: versatile supports in heterogeneous catalysis for liquid phase catalytic transformations. *RSC Adv.*, **2015**, *5*, 24363-24391. https://doi.org/10.1039/C4RA13077D

46 Witzke, R. J.; Chapovetsky, A.; Conley, M. P.; Kaphan, D. M.; Delferro, M. Nontraditional Catalyst Supports in Surface Organometallic Chemistry. *ACS Catal.*, **2020**, *10(20)*, 11822-11840. https://doi.org/10.1021/acscatal.0c03350

47 Liang, J.; Liang, Z.; Zou, R.; Zhao, Y. Heterogeneous Catalysis in Zeolites, Mesoporous Silica, and Metal–Organic Frameworks. *Adv. Matter.*, **2017**, *29*, 1701139. https://doi.org/10.1002/adma.201701139

48 Chongdar, S.; Bhattacharjee, S.; Bhanja, P.; Bhaumik, A. Porous organic–inorganic hybrid materials for catalysis, energy and environmental applications. *Chem. Commun.*, **2022**, *58*, 3429-3460. https://doi.org/10.1039/D1CC06340E

49 Sharma, J.; Plizos, G. Hollow Silica Particles: Recent Progress and Future Perspectives. *Nanomaterials*, **2020**, *10(8)*, 1599. https://doi.org/10.3390/nano10081599

50 Coperet, C.; Comas-Vives, A.; Conley, M. P.; Estes, D. P.; Fedorov, A.; Mougel, V.; Nagae, H.; Nunez-Zarur, F.; Zhizhko, P. A. Surface Organometallic and Coordination Chemistry toward Single-Site Heterogeneous Catalysts: Strategies, Methods, Structures, and Activities. *Chem. Rev.*, **2016**, *116(2)*, 323-421. https://doi.org/10.1021/acs.chemrev.5b00373

51 Gates, B. C.; Flytzani-Stephanopoulos, M.; Dixon, D. A.; Katz, A. Atomically dispersed supported metal catalysts: perspectives and suggestions for future research. *Catal. Sci. Technol.*, **2017**, *7(19)*, 4259-4275. https://doi.org/10.1039/C7CY00881C

52 Reina, A.; Carmona-Chávez, R.; Pulido-Díaz, I. T.; Martínez, D.; Salas-Martin, K. P.; Guerrero-Ríos, I. Silica-Supported 1st Row Transition Metal (Nano)Catalysts: Synthetic and Catalytic Insight. *ChemCatChem*, **2023**, *15(11)*, e202300285. https://doi.org/10.1002/cctc.202300285

53 Pulido-Díaz, I. T.; Serrano-Maldonado, A.; López-Suárez, C. C.; Méndez-Ocampo, P. A.; Portales-Martínez, B.; Gutiérrez-Alejandre, A.; Salas-Martin, K. P.; Guerrero-Ríos, I. RhNPs supported on N-functionalized mesoporous silica: effect on catalyst stabilization and catalytic activity. *Dalton Trans.*, **2021**, *50*, 3289-3298. https://doi.org/10.1039/D0DT04213G

54 Luska, K. L.; Bordet, A.; Tricard, S.; Sinev, I.; Grünert, W.; Chaudret, B.; Leitner, W. Enhancing the Catalytic Properties of Ruthenium Nanoparticles-SILP Catalysts by Dilution with Iron.

ACS Catal. **2016**, *6*, 6, 3719–3726. https://doi.org/10.1021/acscatal.6b00796

55 Rengshausen, S.; Van Stappen, C.; Levin, N.; Tricard, S.; Luska, K. L.; DeBeer, S.; Chaudret, B.; Bordet, A.; Leitner, W. Organometallic Synthesis of Bimetallic Cobalt-Rhodium Nanoparticles in Supported Ionic Liquid Phases (Co$_x$Rh$_{100-x}$@SILP) as Catalysts for the Selective Hydrogenation of Multifunctional Aromatic Substrates. *Small* **2021**, *17(5)*, 2006683. https://doi.org/10.1002/smll.202006683

56 Paschoal, V. H.; Faria, L. F. O.; Ribeiro, M. C. C. Vibratonal Spectroscopy of Ionic Liquids. *Chem. Rev.*, **2017**, *117(10)*, 7053–7112. https://doi.org/10.1021/acs.chemrev.6b00461

57 Protsak, I. S.; Morozov, Y. M.; Dong, W.; Le, Z.; Zhang, D.; Henderson, I. M. A ^{29}Si, ^{1}H, and ^{13}C Solid-State NMR Study on the Surface Species of Various Depolymerized Organosiloxanes at Silica Surface. *Nanoscale Res. Lett.*, **2019**, *14*, 160. https://doi.org/10.1186/s11671-019-2982-2

58 Duong, N. T.; Trébosc, J.; Lafon, O.; Amoureux, J.-P. Improved Sensitivity and Quantification for 29Si NMR Experiments on Solids Using UDEFT (Uniform Driven Equilibrium Fourier Transform). *Solid State Nuclear Magnetic Resonance* **2019**, *100*, 52–62. https://doi.org/10.1016/j.ssnmr.2019.03.007

59 Wang, X.; Cheng, S.; Chan, J. C. C. Propylsulfonic Acid-Functionalized Mesoporous Silica Synthesized by in Situ Oxidation of Thiol Groups under Template-Free Condition. *J. Phys. Chem. C*, **2007**, *111(5)*, 2156-2164. https://doi.org/10.1021/jp066924b

60 Cleare, M. J.; Griffith, W. P. Infrared spectra of isotopically substituted nitro-, nitrito-, and nitrosyl complexes. *J. Chem. Soc. A*, **1967**, *0*, 1144-1147. https://doi.org/10.1039/J19670001144

61 Schneider, P. Adsorption isotherms of microporous-mesoporous solids revisited. *Appl. Catal. A-Gen.* **1995**, *129 (2)*, 157–165. https://doi.org/10.1016/0926-860X(95)00110-7

62 Thommes, M.; Kaneko, K.; Neimark, A. V.; Oliver, J. P.; Rodríguez-Reinoso, F.; Rouquerol, J.; Sing, K. S. W. Physisorption of gases, with special reference to the evaluation of surface area and pore size distribution (IUPAC Technical Report). *Pure Appl. Chem.,* **2015**, *87*, 1051–1069. https://doi.org/10.1515/pac-2014-1117

63 Zhu, L.; Ye, S.; Zhu, J.; Duan, C.; Li, K.; He, G.; Liu, X. Tartaric Acid-Assisted Synthesis of Well-Dispersed Ni Nanoparticles Supported on Hydroxyapatite for Efficient Phenol Hydrogenation. *ACS Sustainable Chem. Eng.*, **2022**, *10*, 10526-10536. https://doi.org/10.1021/acssuschemeng.2c01642

64 Nugent, T. C.; El-Shazly, M. Chiral Amine Synthesis – Recent Developments and Trends for Enamide Reduction, Reductive Amination, and Imine Reduction. *Adv. Synth. Catal.*, **2010**, *352(5)*, 753-819. https://doi.org/10.1002/adsc.200900719

65 Haniti, M.; Hamid, A.; Allen, C. L.; Lamb, G. W.; Maxwell, A. C.; Maytum, H. C.; Watson, A. J., A.; Williams, J. M. J. Ruthenium-Catalyzed *N*-Alkylation of Amines and Sulfonamides Using Borrowing Hydrogen Methodology. *J. Am. Chem. Soc.*, **2009**, *131*, 1766-1774. https://doi.org/10.1021/ja807323a

66 Jumde, V. R.; Petricci, E.; Petrucci, C.; Santillo, N.; Taddei, M.; Vaccaro, L. Domino Hydrogenation–Reductive Amination of Phenols, a Simple Process To Access Substituted Cyclohexylamines. *Org. Lett.*, **2015**, *17*, 3990-3993. https://doi.org/10.1021/acs.orglett.5b01842

67 Zheng, B.; Song, J. Wu, H.; Han, S.; Zhai, J.; Zhang, K.; Wu, W.; Xu, C.; He, M.; Han, B. Palladium-catalyzed synthesis of 4-cyclohexylmorpholines from reductive coupling of aryl ethers and lignin model compounds with morpholines. *Green Chem.*, **2021**, *23*, 268-273. https://doi.org/10.1039/D0GC03188G

68 Zheng, B.; Wu, H.; Song, J.; Wu, W.; Mei, X.; Zhang, K.; Xu, C.; Xu, J.; He, M.; Han, B. Production of alkoxyl-functionalized cyclohexylamines from lignin-derived guaiacols. *Green Chem.*, **2021**, *23*, 8441-8447. https://doi.org/10.1039/D1GC02790E

69 Chen, Z.; Zeng, H.; Gong, H.; Wang, H.; Li, C.-J. Palladium-catalyzed reductive coupling of phenols with anilines and amines: efficient conversion of phenolic lignin model monomers and analogues to cyclohexylamines. *Chem. Sci.*, **2015**, *6*, 4174-4178. https://doi.org/10.1039/C5SC00941C

70 Bragonia, V.; Rit, R. K.; Kirchmann, R.; Trita, A. S.; Goossen, L. J. Synthesis of bio-based surfactants from cashew nutshell liquid in water. *Green Chem.*, **2018**, *20*, 3210-3213. https://doi.org/10.1039/C8GC01686K

71 Lohr, T. L.; Li, Z.; Assary, R. S.; Curtiss, L. A.; Marks, T. J. Thermodynamically Leveraged Tandem Catalysis for Ester RC(O)O–R' Bond Hydrogenolysis. Scope and Mechanism. *ACS Catal.*, **2015**, *5(6)*, 3675-3679. https://doi.org/10.1021/acscatal.5b00950

72 Yan, L.; Liu, X.-X.; Fu, Y. *N*-Alkylation of amines with phenols over highly active heterogeneous palladium hydride catalysts. *RSC Adv.*, **2016**, *6*, 109702-109705. https://doi.org/10.1039/C6RA22383D

73 Cuypers, T.; Morias, T.; Windels, S.; Marquez, C.; Van Goethem, C.; Vankelecom, I.; De Vos, D, E. Ni-Catalyzed reductive amination of phenols with ammonia or amines into cyclohexylamines. *Green Chem.*, **2020**, *22*, 1884-1893. https://doi.org/10.1039/C9GC02625H

74 Ortega, M.; Manrique, R.; Jiménez, R.; Parreño, M.; Domine, M. E.; Arteaga-Pérez, L. E. Secondary Amines from Catalytic Amination of Bio-Derived Phenolics over Pd/C and Rh/C: Effect of Operation Parameters. *Catalysts*, **2023**, *13(4)*, 654. https://doi.org/10.3390/catal13040654

75 Chaudhari, C.; Sato, K.; Rumi, S.; Nishida, Y.; Shiraishi, M.; Nagaoka, K. Rh-PVP Catalyzed Reductive Amination of Phenols by Ammonia or Amines to Cyclohexylamines under Solvent-free Conditions. *Chem. Lett.*, **2022**, *51(1)*, 81-84. https://doi.org/10.1246/cl.210574

76 Mévellec, V.; Nowicki, A.; Roucoux, A.; Dujardin, C.; Granger, P.; Payen, E.; Philippot, K. A simple and reproducible method for the synthesis of silica-supported rhodium nanoparticles and their investigation in the hydrogenation of aromatic compounds. *New J. Chem.*, **2006**, *30*, 1214-1219. https://doi.org/10.1039/B605893K

77 Llop Castelbou, J.; Bresó-Femenia, E.; Blondeau, P.; Chaudret, B.; Castillón, S.; Claver, C.; Godard, C. Tuning the Selectivity in the Hydrogenation of Aromatic Ketones Catalyzed by Similar Ruthenium and Rhodium Nanoparticles. *ChemCatChem*, **2014**, *6(11)*, 3160-3168. https://doi.org/10.1002/cctc.201402524

78 Bagal, D. B.; Bhanage, B. M. Recent Advances in Transition Metal-Catalyzed Hydrogenation of Nitriles. *Adv. Synth. Catal.*, **2015**, *357*, 883-900. https://doi.org/10.1002/adsc.201400940

79 Formenti, D.; Mocci, R.; Atia, H.; Dastgir, S.; Anwar, M.; Bachmann, S.; Scalone, M.; Junge, K.; Beller, M. A State-of-the-Art Heterogeneous Catalyst for Efficient and General Nitrile Hydrogenation. *Chem. Eur. J.*, **2020**, *26*, 15589-15595. https://doi.org/10.1002/chem.202001866

80 Liu, F.; Audemar, M.; De Oliveira Vigier, K.; Clacenc, J.-M.; De Campo, F.; Jérome, F. Combination of Pd/C and Amberlyst-15 in a single reactor for the acid/hydrogenating catalytic conversion of carbohydrates to 5-hydroxy-2,5-hexanedione. *Green Chem.*, **2014**, *16*, 4110-4114. https://doi.org/10.1039/C4GC01158A

81 Nakagawa, Y.; Tamura, M.; Tomishige, K. Catalytic Reduction of Biomass-Derived Furanic Compounds with Hydrogen. *ACS Catal.*, **2013**, *3*, 2655-2668. https://doi.org/10.1021/cs400616p

82 Hronec, M.; Fulajtarova, K.; Liptaj, T. Effect of catalyst and solvent on the furan ring rearrangement to cyclopentanone.

Appl. Catal. A Gen., **2012**, *437-438*, 104-111. https://doi.org/10.1016/j.apcata.2012.06.018

83 Reyes, P.; Salinas, D.; Campos, C.; Oportus, M. Murcia, J.; Rojas, H.; Borda, G.; Fierro, J. L. G. Selective hydrogenation of furfural on Ir/TiO2 catalysts. *Quim. Nova*, **2010**, *33*, 777-780. https://doi.org/10.1590/S0100-40422010000400002

84 Yu, W.; Tang, Y.; Mo, L.; Chen, P.; Lou, H.; Zheng, X. One-step hydrogenation–esterification of furfural and acetic acid over bifunctional Pd catalysts for bio-oil upgrading. *Bioresour. Technol.*, **2011**, *102*, 8241-8246. https://doi.org/10.1016/j.biortech.2011.06.015

85 Ordomsky, V. V.; Schouten, J. C.; Van der Schaaf, J.; Nijhuis, T. A. Biphasic single-reactor process for dehydration of xylose and hydrogenation of produced furfural. *Appl. Catal. A Gen.*, **2013**, *451*, 6-13. https://doi.org/10.1016/j.apcata.2012.11.013

86 Lee, S. P.; Chen, Y. W. Selective Hydrogenation of Furfural on Ni−P, Ni−B, and Ni−P−B Ultrafine Materials. *Ind. Eng. Chem. Res.*, **1999**, *38*, 2548-2556. https://doi.org/10.1021/ie990071a

87 Audemar, M.; Ciotonea, C. De Oliveira Vigier, K.; Royer, S.; Ungureanu, A.; Dragoi, B.; Dumitriu, E.; Jérome, F. Selective Hydrogenation of Furfural to Furfuryl Alcohol in the Presence of a Recyclable Cobalt/SBA-15 Catalyst. *ChemSusChem*, **2015**, *8*, 1885-1891. https://doi.org/10.1002/cssc.201403398

88 Neeli, C. K. P.; Chung, Y.-M.; Ahn, W.-S. Catalytic Transfer Hydrogenation of Furfural to Furfuryl Alcohol by using Ultrasmall Rh Nanoparticles Embedded on Diamine-Functionalized KIT-6. *ChemCatChem*, **2017**, *9*, 4570-4579. https://doi.org/10.1002/cctc.201701037

89 Migowski, P.; Lozano, P.; Dupont, J. Imidazolium based ionic liquid-phase green catalytic reactions. *Green Chem.*, **2023**, *25(4)*, 1237-1260. https://doi.org/10.1039/D2GC04749G

90 Sleigh, C.; Pijpers, A. P.; Jaspers, A.; Coussens, B.; Meier, R. J. On the Determination of Atomic Charge via ESCA Including Application to Organometallics. *Journal of Electron Spectroscopy and Related Phenomena* **1996**, *77* (1), 41–57. https://doi.org/10.1016/0368-2048(95)02392-5

91 Digimizer 4.6.1, MedCalc Software, Belgium, 2005–2012.

92 DigitalMicrograph 3.30.2017.0, Gatan Inc., 1996–2018.

93 Dennis, A. M.; Howard, R. A.; Kadish, K. M.; J. L. Bear, J. Brace and N. Winograd, X-Ray Photoelectron Spectra of Some Dirhodium Carboxylate Complexes. *Inorganica Chim. Acta*, **1980**, *44*, 139–141. https://doi.org/10.1016/S0020-1693(00)90981-2

94 Carvalho, M.; Wieserman, L. F.; Hercules, D. M. Spectroscopic Characterization of Wilkinson's Catalyst Using X-ray Photoelectron Spectroscopy (ESCA). *Appl. Spectrosc.*, **1982**, *36*, 290–296.

95 Abe, Y.; Kato, K.; Kawamura, M.; Sasaki, K. Rhodium and Rhodium Oxide Thin Films Characterized by XPS. *Surf. Sci. Spectra*, **2001**, *8*, 117–125. https://doi.org/10.1116/11.20010801

96 Massiot, D.; Fayon, F.; Capron, M.; King, I.; Le Calvé, S.; Alonso, B.; Durand, J.-O.; Bujoli, B.; Gan, Z.; Hoatson, G. Modelling one- and two-dimensional solid-state NMR spectra. *Magn. Reson. Chem.*, **2002**, *40*, 70-76. https://doi.org/10.1002/mrc.984

97 Uson, R.; Oro, L. A.; Cabeza, J. A.; Bryndza, H. E. Stepro, M. P. Dinuclear Methoxy, Cyclooctadiene, and Barrelene Complexes of Rhodium(I) and Iridium(I). *Inorg. Synth.*, **1985**, *23*, 126–130. https://doi.org/10.1002/9780470132548.ch25

98 Singh, G.; Rani, S.; Saroa, A.; Promila; Arora, A.; Choquesillo-Lazarte, D. Amide-tethered organosilatranes: Syntheses, structural characterization and photophysical properties. *Inorganica Chim. Acta*, **2015**, *433*, 78-91. https://doi.org/10.1016/j.ica.2015.04.034

99 Brünig, J.; Csendes, Z.; Weber, S.; Gorgas, N.; Bittner, R. W.; Limbeck, A.; Bica, K.; Hoffmann, H. Kirchner, K. Chemoselective Supported Ionic-Liquid-Phase (SILP) Aldehyde Hydrogenation Catalyzed by an Fe(II) PNP Pincer Complex. *ACS Catal.*, **2018**, *8(2)*, 1048−1051. https://doi.org/10.1021/acscatal.7b04149

100 Zhao, D.; Huo, Q.; Feng, J.; Chmelka, B., F.; Stucky, G. D. Nonionic Triblock and Star Diblock Copolymer and Oligomeric Surfactant Syntheses of Highly Ordered, Hydrothermally Stable, Mesoporous Silica Structures. *J. Am. Chem. Soc.*, **1998**, *120(24)*, 6024–6036. https://doi.org/10.1021/ja974025i].
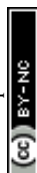
Prof. Dirk Guldi
Editor-in-chief
Nanoscale

June 19th, 2024

Dear Prof. Guldi:

The data supporting this article have been included as part of the Supplementary Information.

Title: "Biomass-derived substrates hydrogenation over Rhodium Nanoparticles Supported on Functionalized Mesoporous Silica"

Authors: Israel T. Pulido-Díaz, Draco Martínez, Karla P. Salas-Martin, Benjamín Portales-Martínez, Dominique Agustin, Antonio Reina and Itzel Guerrero-Ríos

Keywords: rhodium nanoparticles • ordered mesoporous silica • supported ionic liquid phase • hydrogenation • biomass valorization

Dr. Itzel Guerrero-Ríos on behalf of all coauthors.